

Limits on phonon information extracted from neutron pair-density functions

Matthias J. Graf, Il-Kyoung Jeong, Daniel L. Starr, and R. H. Heffner
Los Alamos National Laboratory, Los Alamos, New Mexico 87545, USA

(Received 19 June 2002; published 25 August 2003)

We explore the possibility of extracting information about lattice dynamics in simple crystal structures from the neutron pair-density function (PDF) through inverse data analysis. Contrary to the claims by Dimitrov, Louca, and Röder [Phys. Rev. B **60**, 6204 (1999)], and in agreement with recent work by Reichardt and Pintschovius [Phys. Rev. B **63**, 174302 (2001)], we find that the PDF alone is not sufficient for constructing accurate phonon dispersions in the entire Brillouin zone in systems with complex lattice dynamics. However, our numerical simulations show that for monatomic fcc and bcc crystal structures it is, in principle, possible to obtain phonon moments of complex metals as well as phonon frequencies of simple metals within a few percent accuracy.

DOI: 10.1103/PhysRevB.68.064305

PACS number(s): 63.20.-e, 61.12.Bt

I. INTRODUCTION

Our goal in this work is to determine whether it is possible to obtain high-quality information about the phonon dispersion and lattice dynamics over the entire Brillouin zone without having to measure the phonon dispersion in single crystals. This is an important question for materials where no single crystals are available, or when performing measurements at high pressure and high temperature. This work was motivated by the claim of Dimitrov and co-workers¹ that it is possible to extract accurate phonon dispersions by properly modeling the phonon system and applying an inverse data analysis technique to the *measured* neutron pair-density function (PDF). In principle, the PDF contains all the lattice dynamical information, although most of it is lost after the integration over dynamical and directional degrees of freedom is performed. Very recently, Reichardt and Pintschovius² seriously questioned the results of Dimitrov *et al.*,¹ and concluded that the PDF is rather insensitive to the precise shape of the dispersion curves, and, therefore, that there is no hope for extracting lattice vibrations from experimental PDF measurements. Similar concerns were raised by Møller and McGreevy.³

Experimental PDF data obtained from neutron powder diffraction require various corrections to the raw data, which introduce additional errors in the analysis. Thus, in this paper we studied *synthetic* datasets to avoid any ambiguity in the analysis. We tested and utilized standard reverse Monte Carlo⁴ and Levenberg-Marquardt⁵ methods for the inverse analysis of the PDF spectra to determine how much lattice-dynamical information can be recovered. To do that, we generated synthetic PDF datasets for various monatomic fcc and bcc crystal structures from published tables of generalized Born-von Kármán (BvK) force constants.⁶ We used a BvK model to describe the lattice dynamics since it is easy to implement and is well documented in the literature, although it is not the best-suited phonon model for metals. This gave us full control when testing the robustness and accuracy of the inverse analysis methods being used. We emphasize that we wished to determine whether a unique relationship exists between the phonon dispersion and the corresponding PDF of the system, *not* a unique relationship between the force

constants of the phonon model and its dispersion or PDF spectrum.

Our study of the inverse (indirect) problem of extracting phonons from a given PDF spectrum complements the previous studies by Reichardt and Pintschovius,² who studied the forward (direct) problem of obtaining a unique PDF spectrum from very different phonon dispersion curves.

II. ANALYSIS

We calculated the PDF spectrum by Fourier transforming the powder-averaged, coherent static structure factor $S(q)$,^{1,7-9}

$$\varrho(r) = \varrho_0 + \frac{1}{2\pi^2 r} \int_0^Q dq q \sin(qr) [S(q) - 1], \quad (1)$$

with atomic number density ϱ_0 . For simplicity, we neglected multiphonon processes (i.e., two-phonon and higher-order processes) in the computation of the diffuse scattering part of $S(q)$.¹⁰ Thus, we assumed that the one-phonon scattering process is the dominant inelastic scattering process in the range of usually *measured* scattering vectors, $q < Q \sim 35\text{--}40 \text{ \AA}^{-1}$. However, as was pointed out earlier,^{2,11,12} one needs to be more careful about multiphonon contributions when comparing with actual experiments.

We fit the synthetic PDF datasets $\varrho_{\text{synth}}(r_i)$ with respect to the force constants of the model by minimizing the function

$$\chi_{\text{pdf}}^2 = \frac{1}{N-F} \sum_{i=1}^N \frac{[\varrho_{\text{synth}}(r_i) - \varrho(r_i)]^2}{\sigma^2(r_i)}, \quad (2)$$

where F is the number of force constants being fitted, and $N \gg F$. The number of spatial points is of the order of $N \sim 1000$, and $\sigma(r_i) = \varepsilon_\sigma \varrho(r_*) r_* / r_i$ is an error estimate for $\varrho_{\text{synth}}(r_i)$.⁹ We use a relative error $\varepsilon_\sigma \approx 0.03$ at the first PDF peak maximum at distance r_* , which is typical for experiments with good neutron counting statistics and proper background corrections. Values as low as $\varepsilon_\sigma \approx 0.01$ are feasible in high-precision diffraction experiments. Since ε_σ enters in Eq. (2) only as an overall scaling factor, none of our results depend on the absolute value of ε_σ . The sums run from just

below the first peak through $r_N=1$ nm. Extending the sum to $r_N=2$ nm does not lead to any significant changes in our results. The model PDF $\varrho(r_i)$ depends implicitly on the phonon dispersion and, thus, on the fitted force constants.

One starts the loop of the fitting procedure with a (small) set of plausible force constants and calculates the phonon frequencies $f(\mathbf{k}s)$ and eigenvectors $\mathbf{e}(\mathbf{k}s)$ on a fine mesh in the Brillouin zone (BZ). The computation of the static structure factor in the one-phonon approximation is straightforward, once the frequencies and eigenvectors are known. Finally, one computes the model PDF by convoluting the static structure factor with the instrumental resolution function of the diffractometer¹³ and compares it with the synthetic PDF. An update of the force constants follows. These steps are repeated until a termination criterion is met, either in the implemented reverse Monte Carlo or Levenberg-Marquardt method. Since the Monte Carlo method is computationally intensive and slow compared to a generalized nonlinear least-squares minimizer, we tested the reverse Monte Carlo method only for models with a small set of fitting parameters.

Next we checked the quality of the resulting phonon dispersions by comparing the second phonon moment f_2 and the phonon dispersion $f(\mathbf{k}s)$ with the synthetic phonon data. The second moment of a monatomic crystal is defined by⁶

$$f_2 = \left(\frac{5}{9N_{\text{BZ}}} \sum_{s=1}^3 \sum_{\mathbf{k} \in \text{BZ}} f^2(\mathbf{k}s) \right)^{1/2}, \quad (3)$$

with wave vector \mathbf{k} , phonon branch index s , and N_{BZ} \mathbf{k} points in the summation over the Brillouin zone.

In order to quantify the goodness of the phonon dispersion, we introduce the merit function

$$\chi_{\text{phon}}^2 = \frac{1}{N_p - F} \sum_{i=1}^{N_p} \frac{[f_{\text{synth}}(\mathbf{k}_i s_i) - f(\mathbf{k}_i s_i)]^2}{\sigma_p^2(\mathbf{k}_i s_i)}, \quad (4)$$

where N_p is the number of phonon frequencies. Their estimated errors σ_p are taken to be 2% of the frequency, but at least 0.04 THz. These are typical error estimates reported for neutron triple-axis spectroscopy experiments.

III. RESULTS

We studied in detail elemental Ni, Ag, Al, Ce, and Pb (fcc), as well as Fe and Nb (bcc). Since we obtained very similar results for Ni and Ag, we will not discuss Ag separately. The results for bcc structures show very similar behavior to the ones with fcc structure. Ni has a simple phonon dispersion typical of monatomic fcc crystals, which can be described very well by including only the first few nearest-neighbor (NN) shells of interatomic force constants in a BvK model. On the other hand, Pb shows a complex dispersion (even when neglecting Kohn anomalies) that requires long-range forces up through 8NN shells in a BvK model. Similarly, Fe is the prototype of a monatomic bcc crystal with a simple phonon dispersion, whereas Nb possesses a very complex dispersion.

For each material we used two very different sets of initial

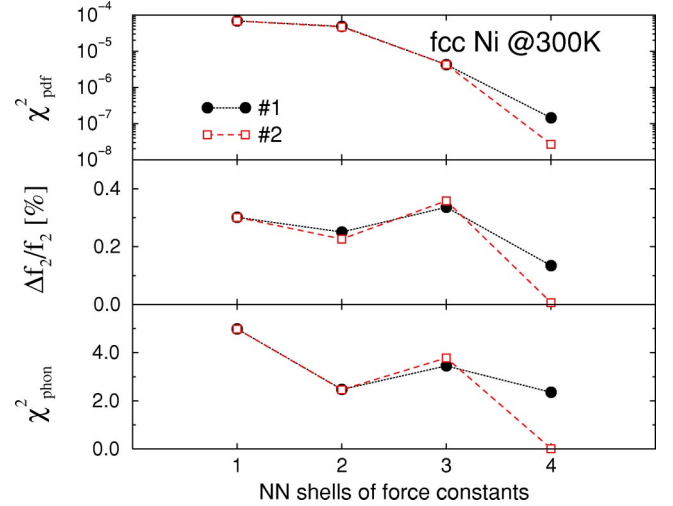


FIG. 1. (Color online) Fitting the synthetic PDF of Ni, generated with a 4NN BvK force model. Top: PDF fits vs number of nearest-neighbor shells of force constants for two different sets (1 and 2). Center: Relative error of f_2 in percent of $f_2^{\text{synth}}=8.03$ THz. Bottom: Figure of merit of computed phonon dispersions shown in Fig. 2.

force constants (sets 1 and 2) to start the fit procedure, in order to test the robustness of the minimization methods. In the fcc simulations shown in Figs. 1–8, we initialized the first shell (1NN) of force constants only (i.e., three parameters), either by using the correct elastic constants (set 1), or by the corresponding values of the 1NN force constants of the synthetic model (set 2). Note that in cubic systems the three independent elastic constants are uniquely defined by three force constants (see the Appendix). In the case of the bcc structures we initialized the combined four force constants of the 1NN and 2NN shells (with the 2NN force constant $XY_2=0$), either by using the correct elastic constants (set 1) or by the corresponding values of the synthetic model (set 2).

Also, for large numbers of force constants the Levenberg-

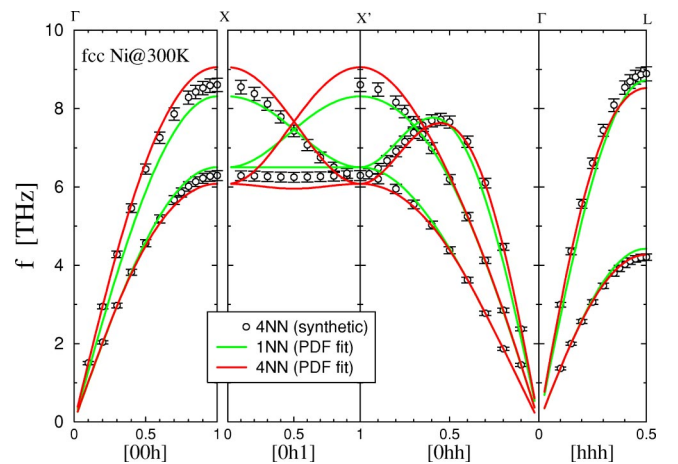


FIG. 2. (Color online) Phonon dispersions along high symmetry directions of the Brillouin zone obtained from fitting the PDF curve of a generalized 4NN BvK force model (Ref. 6), using fit models with 1NN and up to 4NN shells (set 1).

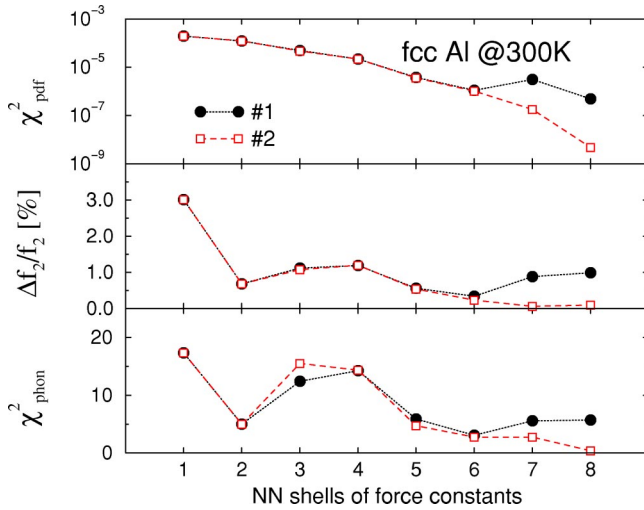


FIG. 3. (Color online) Fitting the synthetic PDF of Al, generated with an 8NN BvK force model. Top: PDF fits vs number of nearest-neighbor shells of force constants for two different sets (1 and 2). Center: Relative error of f_2 in percent of $f_2^{\text{synth}} = 8.28$ THz. Bottom: Figure of merit of computed phonon dispersions shown in Fig. 4

Marquardt algorithm does not always converge to the global minimum. Instead, it gets easily trapped in local minima, depending on the initial values of the force constants. If the initial values are chosen poorly, then this failure is almost unavoidable.

In this section we address in detail the quality and difficulties of fitting the PDF curves and investigate the quality of the corresponding phonon-dispersion curves, phonon moments, elastic constants, Debye-Waller factors, and PDF peak widths for a large set of elemental materials. We show results for systems that range progressively from very simple to very complex phonon models by gradually increasing the number of nearest-neighbor interatomic forces in a Born–Kármán model. In Figs. 1–12 we present a comprehen-

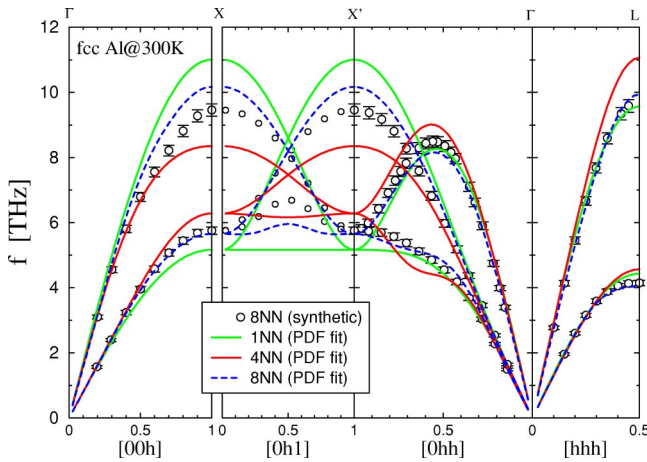


FIG. 4. (Color online) Phonon dispersions obtained from fitting the PDF curve of a generalized 8NN BvK force model (Ref. 6), using fit models with 1NN and up to 4NN and 8NN shells (set 1). Only frequencies (circles) with error bars are included in the computation of χ_{phon}^2 in Fig. 3.

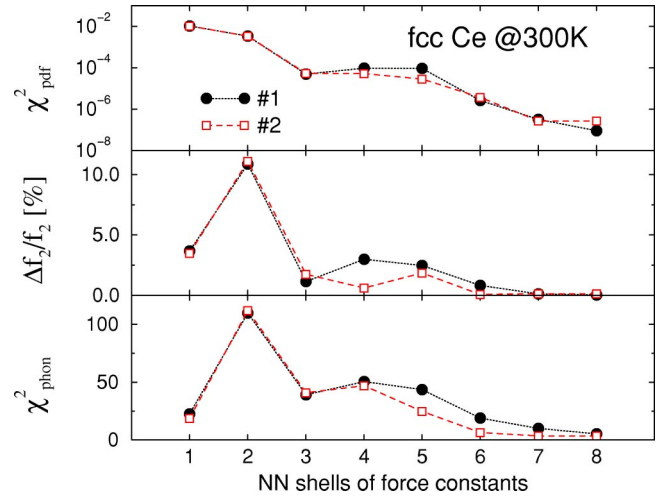


FIG. 5. (Color online) Fitting the synthetic PDF of Ce, generated with an 8NN BvK force model. Top: PDF fits vs number of nearest-neighbor shells of force constants for two different sets (1 and 2). Center: Relative error of f_2 in percent of $f_2^{\text{synth}} = 2.48$ THz. Bottom: Figure of merit of computed phonon dispersions shown in Fig. 6.

sive study of the inverse problem of extracting phonons from PDF curves from elemental cubic materials.

A. Goodness of fit

It is obvious from our results for Ni, Al, Ce, and Pb displayed in Figs. 1–8, and for Fe and Nb in Figs. 9–12, that the PDF is rather insensitive to the zone boundary phonons. This is best seen for the cases of Al, Ce, Pb, and Nb, which have complex phonon dispersions with anomalies close to the Brillouin-zone boundaries. In other words, the PDF is not sensitive enough to register the out-of-phase motions of neighboring atoms.

Also, there is no direct correlation between the goodness of the PDF fit χ_{pdf}^2 and the merit function of the phonon dispersion χ_{phon}^2 . For example, in Fig. 7 it can be seen for the

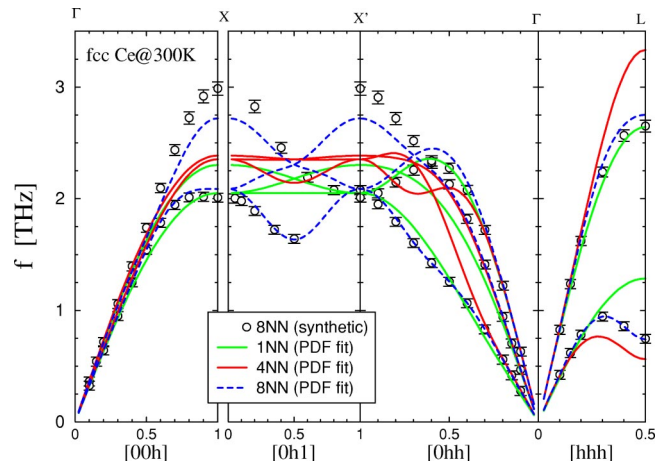


FIG. 6. (Color online) Phonon dispersions obtained from fitting the PDF curve of a generalized 8NN BvK force model (Ref. 6), using fit models with 1NN and up to 4NN and 8NN shells (set 1).

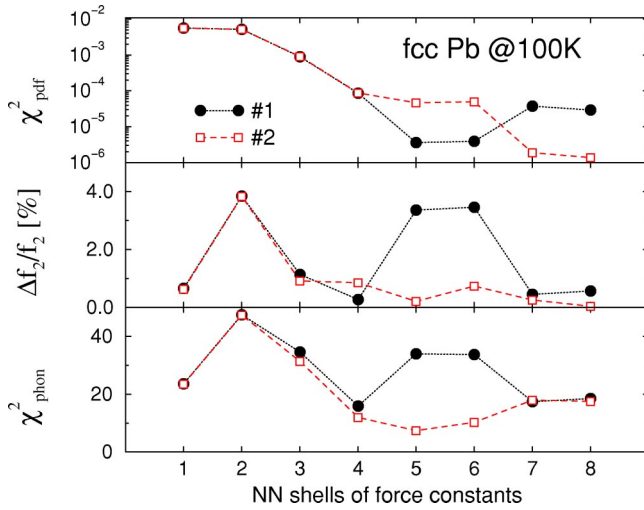


FIG. 7. (Color online) Fitting the synthetic PDF of Pb, generated with an 8NN BvK force model. Top: PDF fits vs number of nearest-neighbor shells of force constants for two different sets (1 and 2). Center: Relative error of f_2 in percent of $f_2^{\text{synth}} = 1.99$ THz. Bottom: Figure of merit of the computed phonon dispersions shown in Fig. 8

metal Pb that χ_{pdf}^2 of set 1 is an order of magnitude smaller than χ_{pdf}^2 of set 2 for 4NN and 5NN BvK models. However, their corresponding χ_{phon}^2 are reversed. This means that a good PDF fit can result in a bad description of the phonon dispersion, and vice versa. Similar conclusions follow from our study of Nb in Fig. 11. This is a very important finding, since it demonstrates the failure of the inverse method because the inverse transformation does not preserve the ordering of the merit function χ_{pdf}^2 . Hence it is generally not possible to provide a useful mapping between PDF spectra and phonon-dispersion curves to solve the inverse problem. We find that χ_{pdf}^2 and χ_{phon}^2 are correlated overall only for simple metals (Ni, Ag, and Fe) and semicomplex metals (Al and

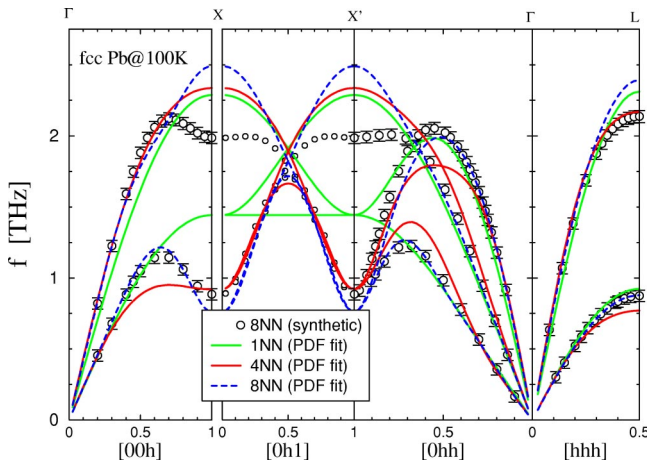


FIG. 8. (Color online) Phonon dispersions obtained from fitting the PDF curve of a generalized 8NN BvK model (Ref. 14), using fit models with 1NN, and up to 4NN and 8NN shells of force constants (set 1). Only frequencies (circles) with error bars are included in the computation of χ_{phon}^2 in Fig. 7.

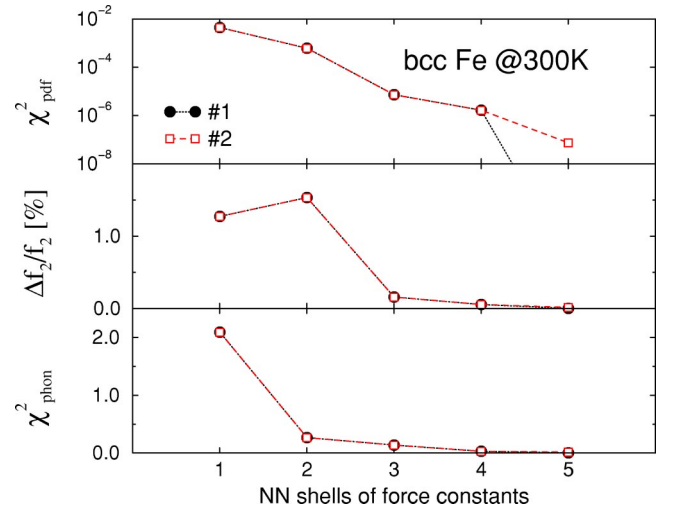


FIG. 9. (Color online) Fitting the synthetic PDF of Fe, generated with a 5NN BvK force model. Top: PDF fits vs number of nearest-neighbor shells of force constants for two different sets (1 and 2). Center: Relative error of f_2 in percent of $f_2^{\text{synth}} = 8.77$ THz. Bottom: Figure of merit of computed phonon dispersions shown in Fig. 10.

Ce), and that both fits improve asymptotically by adding more force constants to the phonon models. This demonstrates that our algorithm successfully solves the inverse problem for simple cases if the PDF spectra can be obtained with arbitrarily high accuracy. At this point it is not clear if this is a robust result that will survive once actual experimental datasets are studied [by including statistical and systematic errors into the computation of $S(q)$]. Thus, it is generally not possible to quantify *a priori* the quality of the extracted phonon dispersions based on χ_{pdf}^2 .

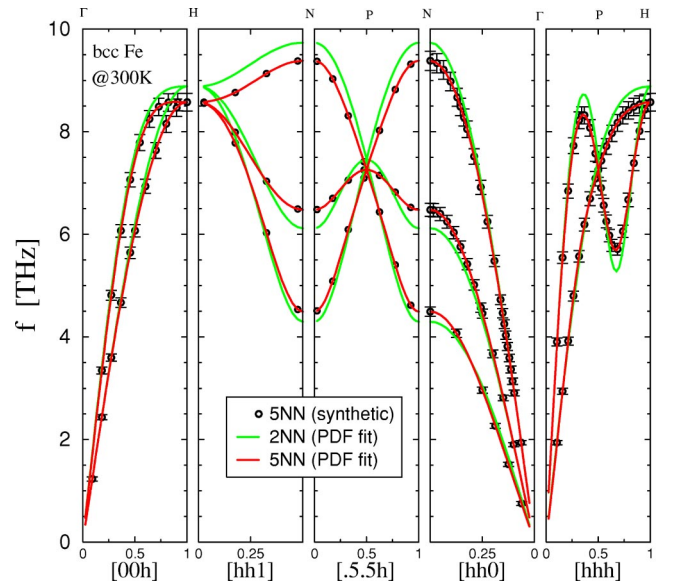


FIG. 10. (Color online) Phonon dispersions obtained from fitting the PDF of a generalized 5NN BvK force model (Ref. 6), using fit models with up to 2NN and 5NN shells (set 1). Only frequencies (circles) with error bars are included in the computation of χ_{phon}^2 in Fig. 9.

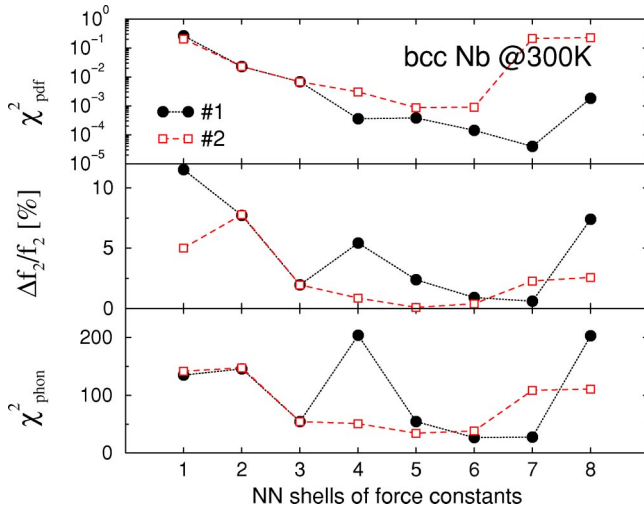


FIG. 11. (Color online) Fitting the synthetic PDF of Nb, generated with an 8NN BvK force model. Top: PDF fits vs number of nearest-neighbor shells of force constants for two different sets (1 and 2). Center: Relative error of f_2 in percent of $f_2^{\text{synth}} = 5.86$ THz. Bottom: Figure of merit of computed phonon dispersions shown in Fig. 12.

All PDF fits to the synthetic datasets are almost indistinguishable, as follows from the extremely small values of χ_{pdf}^2 (see the figures). Note that the smallness of this value depends on the overall scaling factor ε_σ for the accuracy of the *measured* PDF. Only in the controlled analysis of synthetic data has such a small value any significant meaning. This means that even the crudest BvK phonon model with only 1NN interatomic forces deviates on average less than 0.1–1% from the synthetic PDF data, which is in good agreement with the analysis of the *forward* problem in Ref.

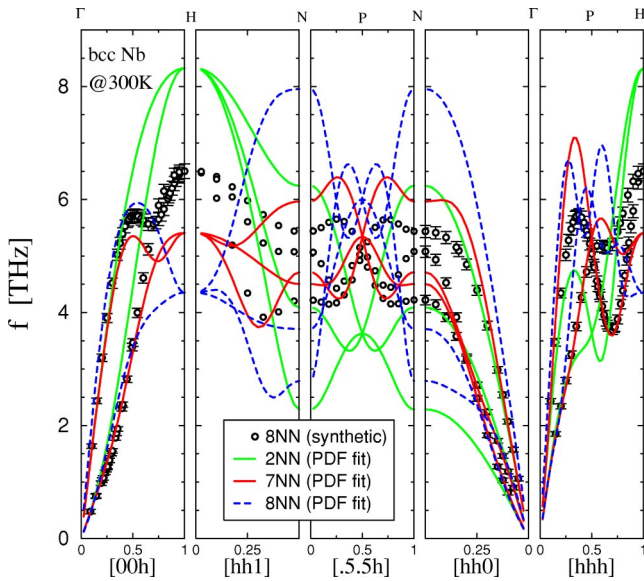


FIG. 12. (Color online) Phonon dispersions obtained from fitting the PDF of a generalized 8NN BvK force model (Ref. 6), using fit models with up to 2NN, 7NN, and 8NN shells (set 1). Only frequencies (circles) with error bars are included in the computation of χ_{phon}^2 in Fig. 11.

2. In any realistic experiment, where statistical and systematic measurement errors may result in a χ_{pdf}^2 of order one, it will be nearly impossible to attribute small reduction of less than 10^{-3} in χ_{pdf}^2 to a significantly improved fit. Hence, in a realistic simulation a PDF fit with a simple 1NN BvK phonon model will be almost indistinguishable from one with a more complex 4NN or 8NN BvK model.

B. Phonon moments

Since phonon moments are an integrated quantity of the phonon-dispersion curves, it is plausible to expect them to be less sensitive to the details of the phonon models being used to generate them. This is indeed the case, as can be seen for the second moment shown in Figs. 1, 3, 5, 7, 9, and 11. Here we focus on the second moment only, because (1) it is more sensitive to high frequencies (near the zone boundaries) than the lower moments, and (2) it enters the free-energy functional in the high-temperature limit, and can be obtained independently in a specific heat measurement. For simple and semicomplex dispersion curves (Ni, Ag, Fe, and Al, Ce) the relative errors of the computed second phonon moments track the overall goodness of the PDF fit. Unfortunately, this is not true for more complex dispersions (Pb and Nb), where we could not establish a correlation between the goodness of χ_{pdf}^2 and the relative error of the second moment ($\Delta f_2/f_2^{\text{synth}} = |f_2 - f_2^{\text{synth}}|/f_2^{\text{synth}}$). However, even systems with complex phonon dispersions allow the extraction of phonon moments within a few percent of accuracy. Several years ago, Knapp *et al.*¹⁵ arrived at similar conclusions while studying the mean-square relative displacement of the central atom in fcc materials with extended x-ray absorption fine-structure measurements.

Finally, our computations for Ce, Pb, and Nb show that the second phonon moment is too insensitive to the phonons at the zone boundaries of the Brillouin zone to be useful for determining zone-boundary phonons.

C. Elastic constants

Dimitrov and co-workers¹ suggested that by adding *measured* elastic constants as constraints to the PDF fit (constrained fit) one can improve upon the extracted phonon dispersions. This is contrary to our own results. We could not observe any significant changes to our extracted phonon dispersions by using constrained PDF fits; i.e., constraining the PDF fit to give force constants that yield the correct elastic constants does not result in better phonon dispersions near the zone boundaries. Of course, it results in slightly more accurate phonon dispersions near the zone center. This is not surprising since the elastic constants determine the long-wavelength limit of the phonon dispersions at the center of the Brillouin zone (Γ point) and not at the zone boundaries, where the discrepancies between the *synthetic* phonon dispersions and the PDF-fitted phonon dispersions are largest. Here the extracted phonon dispersions could improve by providing additional constraints on zone-boundary phonons.

Furthermore, our analysis shows that, in many cases, the unconstrained PDF fits already yield elastic constants that

deviate only a few percent (approximately 1–6%) from the values of the elastic constants of the *synthetic* datasets, when a significantly large number of force constants are being used. By “sufficiently large” we mean at least a 3NN BvK force model for Ni, Ag, Ce, and Fe, and a 5NN BvK model for Al and Pb. This does not work for Nb, however, where the extracted elastic constants are more than 10% off, even for the best fit. For a definition of the elastic constants in terms of a BvK force model for fcc and bcc crystal structures, see the Appendix.

D. Debye-Waller factor

Reichardt and Pintschovius suggested that it might be possible to improve the quality of extracted phonon dispersions by adding constraints to the PDF fit, e.g., thermal parameters independently measured by a Rietveld analysis. The thermal parameters, which are given by the exponent of the Debye-Waller factor, e^{-2W} , measure the mean-square atomic displacement $\langle u^2 \rangle$. For cubic crystals the Debye-Waller exponent simplifies to⁷

$$2W(\mathbf{q}) = \langle (\mathbf{q} \cdot \mathbf{u})^2 \rangle = q^2 \langle u_q^2 \rangle = \frac{1}{3} q^2 \langle u^2 \rangle, \quad (5)$$

where u_q is the component of the displacement vector \mathbf{u} in the direction of the scattering vector \mathbf{q} . This result may be expressed another way,

$$\begin{aligned} W(\mathbf{q}) &= \frac{\hbar}{4MN_{\text{BZ}}} \sum_s \sum_{\mathbf{k} \in \text{BZ}} \frac{|\mathbf{q} \cdot \mathbf{e}(\mathbf{k}s)|^2}{\omega(\mathbf{k}s)} \coth\left(\frac{\hbar\omega(\mathbf{k}s)}{2k_B T}\right) \\ &= \frac{\hbar q^2}{4M} \int_0^\infty d\omega \mathcal{W}(\omega), \end{aligned} \quad (6)$$

with the Debye-Waller spectral function given by

$$\mathcal{W}(\omega) = \frac{N(\omega)}{\omega} \coth\left(\frac{\hbar\omega}{2k_B T}\right), \quad (7)$$

where M is the atomic mass, $\omega(\mathbf{k}s)$ is the angular frequency of mode s , and $\mathbf{e}(\mathbf{k}s)$ is its normalized eigenvector. The phonon density of states is normalized so that

$$\int_0^\infty d\omega N(\omega) = 1, \quad (8)$$

and $N(\omega) \equiv 0$ for ω larger than the maximum phonon frequency.

We used Eq. (6) to compute the thermal parameters in our inverse PDF analysis. The thermal parameters computed from the force constants of the best PDF fits were remarkably insensitive to the specific form of the phonon model. Even for the simplest phonon models used, the relative error of $\langle u^2 \rangle$ was typically less than 1% (less than 0.1% for Ni, Ag, Al, and Pb) and less than 5% for Nb. Thus, measured thermal parameters, whose absolute values are known only within a few percent, cannot give improved PDF fits or better phonon dispersions. Indeed, it is well known that the Debye-Waller (DW) factor is rather insensitive to the detailed form

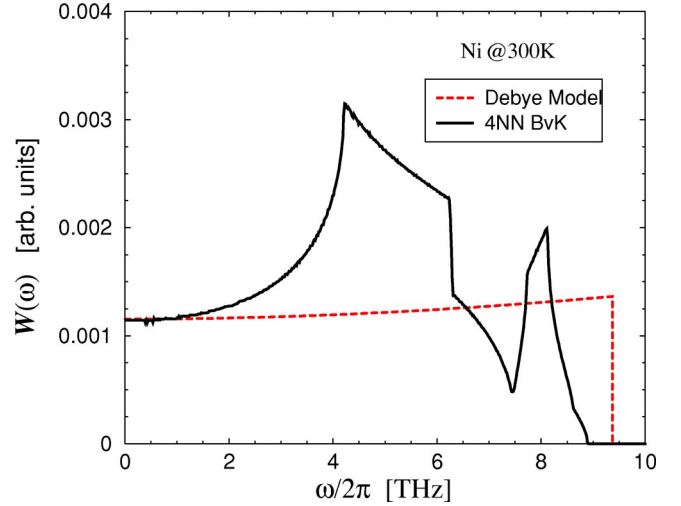


FIG. 13. (Color online) A comparison of the Debye-Waller spectral functions of Ni at 300 K for a realistic 4NN BvK phonon model (Ref. 6) with its corresponding Debye phonon model.

of the phonon dispersion. At high temperatures it depends only on a single parameter, namely, the inverse-squared phonon moment.¹⁶

For those familiar with lattice dynamics, the following observation may be obvious, nevertheless we think that by giving two simple examples we can clarify some of the confusion surrounding various definitions of Debye temperatures and the phonon content in the Debye-Waller factor. Since it is a common practice to compare *so-called* Debye temperatures Θ_{DW} derived from high-temperature Debye-Waller factors, $2W \propto T/\Theta_{\text{DW}}^2$, with Debye temperatures Θ_{D} derived from ultrasound or low-temperature specific-heat data, $\Theta_{\text{D}} \propto \omega_{\text{D}}$, we wish to point out that $\Theta_{\text{D}} \neq \Theta_{\text{DW}}$, except for the special case of a Debye spectrum. When using elastic constants (derived from ultrasound) with a Debye phonon model to estimate Debye-Waller factors, or when comparing Θ_{D} with Θ_{DW} , one usually observes discrepancies of 10–20%. This is not too surprising, because Θ_{D} and Θ_{DW} are related to two very different phonon moments. Figures 13 and 14 illustrate for Ni and Ce that at room temperature the Debye-Waller spectral function $\mathcal{W}(\omega)$, estimated from the elastic modes, is only a crude approximation to the correct spectral function. It consistently underestimates the contribution of the intermediate frequency region (transverse modes near the zone boundary) and describes the high-frequency region (longitudinal modes near the zone boundary) only on average. Here the Debye-Waller exponents $2W$ computed from a Debye phonon model are 20% too small compared to the ones using more realistic lattice-dynamical models. The other materials studied in this work show similar discrepancies, except in the case of Nb where both the Debye and lattice model calculations of the thermal parameters accidentally agree within 1%.

E. PDF peak widths

An important question that remains to be addressed is how much phonon information is actually embedded in the

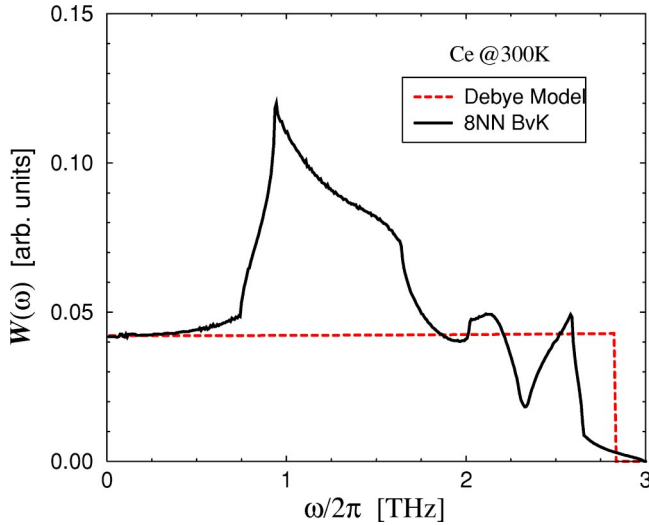


FIG. 14. (Color online) A comparison of the Debye-Waller spectral functions of Ce at 300 K for a realistic 8NN BvK phonon model (Ref. 6) with its corresponding Debye phonon model.

individual PDF peaks. Knowing the answer to this question can significantly constrain the amount of sophistication for a phonon model needed to model realistic PDF spectra. We follow Warren¹⁷ and Chung and Thorpe¹¹ for studying the local atomic structure properties. By using the real-space approach for computing PDF spectra, all multiphonon processes are automatically included. They showed in the harmonic approximation that the PDF $\varrho(r)$ is approximately a series of Gaussian peaks, each centered at distance r_i with width σ_i , i.e.,

$$\varrho(r) \approx \sum_i w_i \exp[-(r - r_i)^2 / 2\sigma_i^2], \quad (9)$$

where the weight factor w_i guarantees the correct coordination number of atoms in each interatomic shell and

$$\sigma_i^2 = \frac{\hbar}{MN_{\text{BZ}}} \sum_s \sum_{\mathbf{k} \in \text{BZ}} \coth\left(\frac{\hbar\omega(\mathbf{k}s)}{2k_B T}\right) \times \frac{|\hat{r}_i \cdot \mathbf{e}(\mathbf{k}s)|^2}{\omega(\mathbf{k}s)} [1 - \cos(\mathbf{k} \cdot \mathbf{r}_i)]. \quad (10)$$

Here \mathbf{r}_i is a position vector of an atom in the i th NN interatomic shell measured relative to an atom at the origin, and $\hat{r}_i = \mathbf{r}_i / r_i$. In the limit $\mathbf{k} \cdot \mathbf{r}_i \gg 1$, the cosine term oscillates so rapidly across the BZ that its average vanishes and the peak widths of far-out atoms contain the same information as the Debye-Waller exponent, namely, $\lim_{i \rightarrow \infty} \sigma_i^2 \equiv \sigma_\infty^2 = 4W(q)/q^2$. This explains our results in the preceding section on why the inverse PDF fits reproduced the Debye-Waller factors so well, and why adding thermal parameters to the fitting procedure would not provide any extra constraints.

Since far-neighbor atom PDF peaks do not contain information beyond the Debye-Waller factor, we focus on the phonon content of the near-neighbor PDF peaks. In particular, we investigate the 1NN PDF peak. Because of the cor-

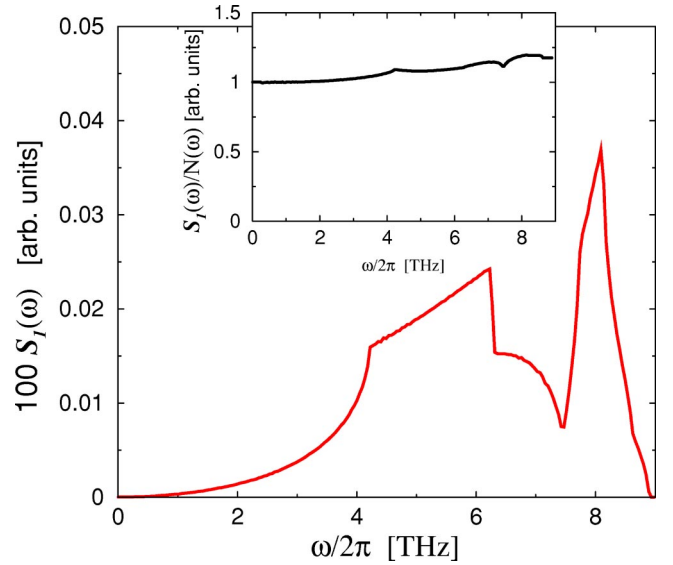


FIG. 15. (Color online) The spectral function of the first PDF peak of Ni at 300 K. Inset: $S_1(\omega)/N(\omega)$ is nearly constant for frequencies $\omega < \omega_{\text{max}}/3$, with $\omega_{\text{max}} \approx 8.9$ THz.

related atomic motion of nearest neighbors, this peak width deviates most significantly from the far-neighbor value σ_∞ . Therefore, the 1NN peak is the most promising peak for deconvoluting the embedded phonon information. Expanding $\cos(\mathbf{k} \cdot \mathbf{r}_i)$ in Eq. (10), it can be shown that at high temperatures and for low frequencies the spectral function of σ_1^2 is, in first-order approximation, dominated by the phonon density of states. Let us define the spectral function $S_i(\omega)$ of the i th peak as

$$\sigma_i^2 = \frac{\hbar}{M} \int_0^\infty d\omega S_i(\omega), \quad (11)$$

$$S_i(\omega) = \mathcal{W}(\omega) \langle |\hat{r}_i \cdot \mathbf{e}(\mathbf{k}s)|^2 [1 - \cos(\mathbf{k} \cdot \mathbf{r}_i)] \rangle_\omega, \quad (12)$$

where $\langle \dots \rangle_\omega$ is a normalized average over phonon modes and \mathbf{k} points at fixed frequency, $\omega(\mathbf{k}s) = \omega$, and $S_i(\omega) \equiv 0$ for frequencies larger than the maximum phonon frequency. It is important to realize that because of this average the spectral function $S_i(\omega)$ in Eq. (12) contains additional lattice-dynamical information compared to the Debye-Waller spectral function $\mathcal{W}(\omega)$ in Eq. (7). For sufficiently small frequencies, we obtain in leading order $\langle |\hat{r}_i \cdot \mathbf{e}(\mathbf{k}s)|^2 [1 - \cos(\mathbf{k} \cdot \mathbf{r}_i)] \rangle_\omega \sim k^2 a^2 \sim (a/c)^2 \omega^2$, with the average sound speed c and lattice constant a . Note that this approximation is equivalent to an isotropic Debye approximation with $\Theta_D \propto c$. For temperatures $T \gg \hbar\omega/2k_B$, the width of the first peak is proportional to the integrated phonon density of states (which is unity) times $(\hbar/M)(a^2/c^2)$, as can be seen in the insets of Figs. 15 and 16, where $S_1(\omega)$ tracks closely $N(\omega)$. Using the approximate form of the average to calculate the 1NN PDF peak width for Ni and Ce, we find that it differs by a few percent from the exact value of σ_1 , respectively. Such small deviations, due to the full knowledge of the phonon dispersion, are very difficult to be picked up in any *real* PDF experiment. A similar result was found in the extensive PDF

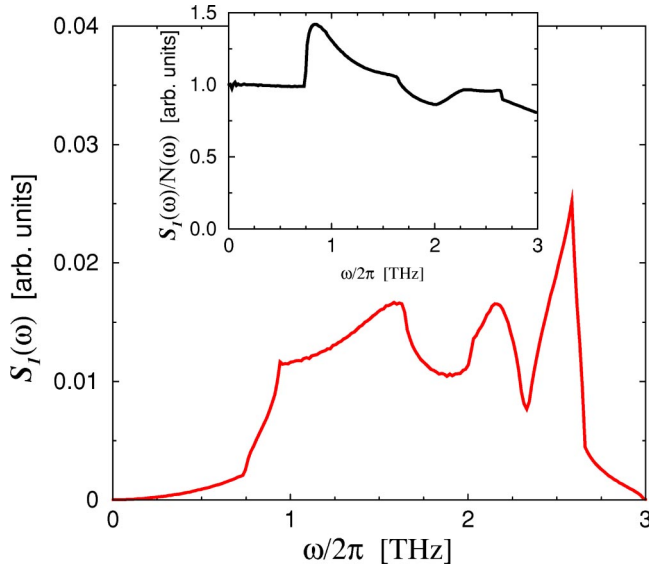


FIG. 16. (Color online) The spectral function of the first PDF peak of Ce at 300 K. Inset: $S_1(\omega)/N(\omega)$ is nearly constant for frequencies $\omega < \omega_{\max}/4$, with $\omega_{\max} \approx 3.0$ THz.

study by Jeong and co-workers,¹⁸ who compared experimental PDF measurements with BvK and correlated Debye model calculations.

The key results of this section are (1) that there is little lattice-dynamical information in the PDF peak widths, which goes beyond the Debye model, and (2) that at high temperatures the width of the 1NN PDF peak is related to Θ_D , $\sigma_1^2 \propto T/\Theta_D^2$, whereas the thermal parameter or σ_z^2 is related to Θ_{DW} , $\sigma_z^2 \propto T/\Theta_{DW}^2$.

IV. CONCLUSIONS

In conclusion, our study shows that one cannot obtain accurate phonon dispersions from an inverse analysis of the pair-density function, unless the lattice dynamics is simple and fully described by a few phonon parameters, as in the cases of fcc Ni and Ag and bcc Fe, for example. A semiquantitative picture of the phonon dispersion may be obtained in simple and semicomplex metals, but not in metals with complex phonon dispersions. In principle, in simple metals phonon frequencies can be extracted within a few percent accuracy (~ 2 – 8%) in the entire Brillouin zone, whereas in semicomplex and complex metals such accuracy applies only to a small fraction of the Brillouin zone centered around the Γ point with wave vector $k \lesssim \pi/4a$. Unfortunately, these are *a posteriori* results and one never knows *a priori* whether a material has a simple or complex phonon dispersion.

We found numerically that the pair-density function provides an overall account of the lattice dynamics by yielding phonon moments within a few percent accuracy. In other words, a rather simple phonon model suffices to describe the lattice dynamics embedded in powder diffraction data. Neutron or x-ray PDF studies play an important role in the studies of the local structure of crystals, but cannot provide deeper insight into the dynamics of lattice vibrations. A more promising approach for extracting phonons from powders or

TABLE I. Symmetries of the generalized BvK force constant matrix Φ_{nNN} for monatomic fcc and bcc crystal structures. The lattice indices $[h_1 h_2 h_3]$ refer to lattice positions $(h_1, h_2, h_3)a/2$ with $h_1 \geq h_2 \geq h_3$.

Shell	fcc	bcc
1NN	[110] $XX_1 = YY_1$ $XZ_1 = YZ_1 = 0$	[111] $XX_1 = YY_1 = ZZ_1$ $XY_1 = XZ_1 = YZ_1$
2NN	[200] $YY_2 = ZZ_2$ $XY_2 = XZ_2 = YZ_2 = 0$	[200] $YY_2 = ZZ_2$ $XY_2 = XZ_2 = YZ_2 = 0$
3NN	[211] $YY_3 = ZZ_3$ $XY_3 = XZ_3$	[220] $XX_3 = YY_3$ $XZ_3 = YZ_3 = 0$
4NN	[220] $XX_4 = YY_4$ $XZ_4 = YZ_4 = 0$	[311] $YY_4 = ZZ_4$ $XY_4 = XZ_4$
5NN	[310] $XZ_5 = YZ_5 = 0$ –	[222] $XX_5 = YY_5 = ZZ_5$ $XY_5 = XZ_5 = YZ_5$
6NN	[222] $XX_6 = YY_6 = ZZ_6$ $XY_6 = XZ_6 = YZ_6$	[400] $YY_6 = ZZ_6$ $XY_6 = XZ_6 = YZ_6 = 0$
7NN	[321] –	[331] $XX_7 = YY_7, XZ_7 = YZ_7$
8NN	[400] $YY_8 = ZZ_8$ $XY_8 = XZ_8 = YZ_8 = 0$	[420] $XZ_8 = YZ_8 = 0$

polycrystals may be the analysis of time-of-flight spectra from inelastic neutron scattering.^{19,20}

ACKNOWLEDGMENTS

We thank D. Wallace, A. Lawson, H. Röder, L. Pintschovius, D. Strauch, and G. Eckold for many helpful discussions, and especially J. Wills for helping with the symmetry operations and \mathbf{k} -point summations. This work was supported by the Los Alamos National Laboratory under the auspices of the U. S. Department of Energy.

APPENDIX: ELASTIC CONSTANTS IN A BORN–VON KÁRMÁN FORCE MODEL

In a cubic crystal there are only three independent elastic constants.²¹ For fcc crystal structures with lattice constant a , these are related to the force constants (up through 8NN interatomic shells) by

$$\begin{aligned}
 aC_{11} = & 4XX_1 + 4XX_2 + 16XX_3 + 8YY_3 + 16XX_4 + 36XX_5 \\
 & + 4YY_5 + 16XX_6 + 72XX_7 + 32YY_7 + 8ZZ_7 + 16XX_8,
 \end{aligned}
 \tag{A1}$$

$$aC_{44} = 2XX_1 + 2ZZ_1 + 4YY_2 + 4XX_3 + 20YY_3 + 8XX_4 \\ + 8ZZ_4 + 2XX_5 + 18YY_5 + 20ZZ_5 + 16XX_6 + 20XX_7 \\ + 40YY_7 + 52ZZ_7 + 16YY_8, \quad (\text{A2})$$

$$a(C_{12} + C_{44}) = 4XY_1 + 8YZ_3 + 32XZ_3 + 16XY_4 + 24XY_5 \\ + 32YZ_6 + 96XY_7 + 48XZ_7 + 32YZ_7, \quad (\text{A3})$$

and for bcc structures these are given by

$$aC_{11} = 2XX_1 + 2XX_2 + 8XX_3 + 18XX_4 + 4YY_4 + 8XX_5 \\ + 8XX_6 + 36XX_7 + 2ZZ_7 + 32XX_8 + 8YY_8, \quad (\text{A4})$$

$$aC_{44} = 2XX_1 + 2YY_2 + 4XX_3 + 4ZZ_3 + 2XX_4 + 20YY_4 \\ + 8XX_5 + 8YY_6 + 20XX_7 + 18ZZ_7 + 4XX_8 + 16YY_8 \\ + 20ZZ_8, \quad (\text{A5})$$

$$a(C_{12} + C_{44}) = 4XY_1 + 8XY_3 + 4YZ_4 + 24XY_4 + 16XY_5 \\ + 24YZ_7 + 36XY_7 + 32XY_8, \quad (\text{A6})$$

where we followed the derivation of Squires.^{22,23} Our elastic constants agree with those in Ref. 22 where comparison is possible, except for the term $4YY_4$ in C_{11} for bcc structures. The generalized BvK force matrix of the n th NN interatomic shell is defined by

$$\Phi_{n\text{NN}} = \begin{pmatrix} XX_n & XY_n & XZ_n \\ XY_n & YY_n & YZ_n \\ XZ_n & YZ_n & ZZ_n \end{pmatrix}. \quad (\text{A7})$$

Its symmetry properties are listed in Table I.

¹D.A. Dimitrov, D. Louca, and H. Röder, Phys. Rev. B **60**, 6204 (1999).

²W. Reichardt and L. Pintschovius, Phys. Rev. B **63**, 174302 (2001).

³A. Mellergård and R.L. McGreevy, Chem. Phys. **261**, 267 (2000).

⁴A. Corana, M. Marchesi, C. Martini, and S. Ridella, ACM Trans. Math. Softw. **13**, 262 (1987).

⁵W. H. Press, S. A. Teucholsky, W. T. Vetterling, and B. P. Flannery, *Numerical Recipes in C* (Cambridge University Press, Cambridge, England, 1999).

⁶P. H. Dederichs, H. Schober, and D. J. Sellmyer, *Metalle: Phononenzustände und Fermiflächen*, edited by K.-H. Hellwege and J. L. Olsen, Landolt-Bornstein, New Series, Group 3, Vol. 13a (Springer, New York, 1981).

⁷G. L. Squires, *Introduction to the Theory of Thermal Neutron Scattering* (Dover, Mineola, NY, 1996).

⁸S. L. Lovesey, *Theory of Neutron Scattering from Condensed Matter: Nuclear Scattering* (Clarendon Press, Oxford, 1987)

⁹B.H. Toby and T. Egami, Acta Crystallogr., Sect. A: Found. Crystallogr. **48**, 336 (1992).

¹⁰We mimic the effects of multiphonon processes by adding a smooth function, $S_m(q) = 1 - \exp[-2W(q)/2.4]$, to the computation of the coherent static structure factor $S(q) = S_0(q) + S_1(q) + S_m(q)$. In addition to the elastic (S_0) and 1-phonon (S_1) coherent scattering contributions, S_m guarantees the correct asymptotic limits of $S(q)$, namely, $\lim_{q \rightarrow \infty} S(q) = 1$ and $\lim_{q \rightarrow 0} S(q) = 0$.

¹¹J.S. Chung and M.F. Thorpe, Phys. Rev. B **55**, 1545 (1997).

¹²M. F. Thorpe, V. Levashov, M. Lei, and S. J. L. Billinge, in

Proceedings of the Workshop on *From Semiconductors to Proteins: Beyond the Average Structure, 2001*, Traverse City, MI, edited by S. J. L. Billinge and M. F. Thorpe (Kluwer Academic/Plenum, New York, 2001), p. 105.

¹³We used a standard (non-Gaussian) diffractometer resolution function (type I) as specified in the GSAS manual: A. C. Larson and R. B. von Dreele, Los Alamos National Laboratory Report No. LA-UR:86-748, 1986 (unpublished); see also ftp://ftp.lanl.gov/public/gsas/manual.

¹⁴We used a slightly improved set of force constants for Pb, which results in more accurate phonon frequencies near the zone boundaries than the one in Ref. 6.

¹⁵G.S. Knapp, H.K. Pan, and J.M. Tranquada, Phys. Rev. B **32**, 2006 (1985).

¹⁶W. Marshall and S. L. Lovesey, *Theory of Thermal Neutron Scattering* (Clarendon Press, Oxford, 1971), p. 73.

¹⁷B. E. Warren, *X-Ray Diffraction* (Dover, Mineola, NY, 1990), Chap. 11.

¹⁸I.-K. Jeong, R.H. Heffner, M.J. Graf, and S.J.L. Billinge, Phys. Rev. B **67**, 104301 (2003).

¹⁹U. Buchenau *et al.*, Phys. Rev. B **27**, 955 (1983).

²⁰M. Heiroth, U. Buchenau, H.R. Schober, and J. Evers, Phys. Rev. B **34**, 6681 (1986).

²¹D. C. Wallace, *Thermodynamics of Crystals* (Dover, Mineola, NY, 1998), Chap. 2.

²²G. L. Squires, in Proceedings of the symposium on *Inelastic Scattering of Neutrons in Solids and Liquids* (IAEA, Vienna, 1963), Vol. II, p. 71.

²³G.L. Squires, Ark. Fys. **25**, 21 (1962).